ISBN: 978-3-95450-261-5 ISSN: 2673-7000 doi: 10.18429/JACoW-NAPAC2025-WEP092

ULTRA-VIOLET LASER TRANSVERSE SHAPING WITH PHASE PLATES

T. Jogand-Coulomb*, N. Majernik, C. Emma, B. O'Shea, G. Just, A. Osman, T. Xu,
Y. Liu, K. Li, S. Marchesini[1], A. Sakdinawat, N. Burdet, G. Yocky, M. Hogan,
D. Magana, A. Marinelli[1], Z. Huang[1], A. Halavanau†
SLAC National Accelerator Laboratory, Menlo Park, CA, USA
[1]also at Stanford University, Stanford, CA, USA

Abstract

Shaping ultraviolet (UV) laser beams is critical for optimizing photoinjector performance for applications in free-electron lasers (FELs) and beyond. It has been shown that a 50% truncated Gaussian beam can achieve the lowest emittance via space charge compensation at LCLS-I. However, conventional shaping techniques to prepare this beam are limited by significant power losses or are not adapted for UV light. Here we report a high-precision transverse-shaping technique based on custom fused-silica phase plates with >99% transmission at 253 nm. This approach enables spatial beam profile tailoring and significantly enhances beam stability at the photocathode. Using IMPACT-T simulations, we predict a 33% (from 0.67 µm to 0.45 µm) reduction in normalized emittance for a 250 pC bunch at LCLS-I. Experimental implementation at FACET-II demonstrated a 37% emittance reduction (from 5.4 µm to 3.4 µm) at 1.6 nC. These results establish phase-plate beam shaping as a high-fidelity, low-loss approach for high-brightness photoinjectors. Implementation at LCLS-II which will enable stable operation at megahertz repetition rates is underway.

INTRODUCTION

The performance and cost of x-ray free-electron lasers depend critically on transverse emittance of the electron beam [1–6]. It has been shown that for the Linac Coherent Light Source (LCLS-I) the optimal transverse ultraviolet profile at the photocathode to reduce emittance is a Gaussian truncated at 50% [7, 8]. The cost and performance of the FEL depends on stable and reliable beam delivery. There are three major areas of improvement for this at LCLS: (i) refining the transverse profile, (ii) reducing transverse jitter, (iii) reducing charge jitter. Solving these problems would reduce tune-up time significantly and allow for more beam delivery and user experiments.

Despite advances in existing shaping techniques such as spatial light modulators [9, 10] and digital mirror devices [11], these techniques still incur significant power losses or lack compatibility with UV drive wavelengths. Here, we present a high-precision transverse shaping method based on custom fused-silica phase plates designed via an optical Iterative Fourier Transform Algorithm (IFTA) [12]. Our phase plates exhibit greater than 99% transmission at 253 nm, enabling tailored spatial profiles without sacrificing laser energy at the cathode. This method also stabilizes the transverse jitter of the beam at the cathode. We characterize the effectiveness of this technique through Impact-T simulations [13] at LCLS-I and experimental results at FACET-II.

* tcoulomb@slac.stanford.edu
† aliaksei@slac.stanford.edu

SIMULATIONS & THEORY

We implement a custom Fresnel-propagation code to model the transport of a $\lambda = 253$ nm field through our photoinjector optics. We initialize a two-dimensional Gaussian field via the complex q-parameter [14]:

$$\hat{E}(\omega, x, y, 0) = \frac{1}{q(0)} \exp\left[-i\frac{k}{2}\frac{x^2+y^2}{q(0)}\right], \tag{1}$$

where $q = z + iz_R$, $z_R = \frac{\pi\omega_0^2 n}{\lambda}$, $k = \frac{2\pi}{\lambda}$ is the wavenumber and ω_0 is the waist radius. Then we can apply the transfer functions for a lens and propagation through air to propagate the field in space. The lens transfer function [15] is as follows,

$$h_L = \exp\left[-i\frac{k}{2}\frac{x^2+y^2}{f}\right], \tag{2}$$

where f is the focal length of the lens determined by the lens maker equation for a given material with a given radius of curvature. We can apply this transfer function in real space using,

$$\hat{E}(\omega, x, y, 0) \cdot h_L. \tag{3}$$

To propagate through space, we apply the Fresnel propagation transfer function in k-space [16].

$$H_f = \exp\left[iz\sqrt{k^2 - (k_x^2 + k_y^2)}\right] \tag{4}$$

$$\mathscr{F}^{-1}\left[\mathscr{F}\left[\hat{E}(\omega, x, y, 0)\right] \cdot H_f(k_x, k_y, z)\right] \tag{5}$$

To tailor the transverse profile at the photocathode, we design a phase mask using an optical IFTA (Fig.1) which performs the Fourier transforms using an optical propagator to the Fourier plane. This is a variation of the HIOA [12, 17, 18] but keeps the Fourier plane in real space to perform accurate shaping. Starting from a fully randomized phase $\phi_0(x, y)$, each iteration follows in a four step process,

$$E_k = \mathscr{P}\left[|E_{meas}| \exp[i\phi_k]\right], \tag{6}$$

$$\hat{E_k} = |E_{target}| \exp[i\Phi_k], \tag{7}$$

$$E'_k = \mathscr{P}^{-1}\left[|E_{target}| \exp[i\Phi_k]\right] \tag{8}$$

$$E_{k+1} = |E_{meas}| \exp[i\phi_{k+1}]. \tag{9}$$

Here, $\mathscr{P}$ denotes forward Fresnel propagation (lens $+f$ then free-space $+f$) and $\mathscr{P}^{-1}$ its inverse (free-space $-f$ then lens

ISBN: 978-3-95450-261-5 ISSN: 2673-7000 doi: 10.18429/JACoW-NAPAC2025-WEP092

$-f$). Φ_k denotes the phase in the Fourier plane. At each step we quantize ϕ_{k+1} to the discrete phase levels of our fused-silica plate and iterate until the Summed Square Error (SSE) [19] between $|E_{\text{meas}}|^2$ and $|E_{\text{target}}|^2$ converges.

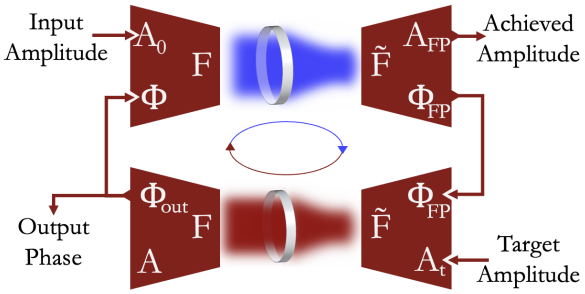

Figure 1: Schematics of the Optical IFTA implemented to generate the phase masks.

After convergence, we extract the final phase map for fabrication and validate its performance by re-propagating through the Fresnel model above. To characterize the speckle of the transverse profile we use the characteristic speckle [20] approach that considers the FWHM of the autocorrelation of the profile's speckle pattern (Eq. 10) to quantify the profile's speckle size. We determine the autocorrelation using the Wiener-Khinchin Theorem as follows,

$$\text{Speckle} = \text{FWHM}\left(\mathscr{F}^{-1}\left[|\tilde{E}|^2\right]\right). \tag{10}$$

To determine the transverse shape we can fit the profile to a truncated Gaussian profile using the following formula,

$$f_T(r) = \begin{cases} A_T \exp\left(-\frac{r^2}{2\sigma^2}\right), & -a < r < a, \\ 0, \text{ elsewhere} \end{cases} \tag{11}$$

$$A_T = \sqrt{\frac{2}{\pi}} \frac{1}{\sigma\left[\text{Erf}\left(\frac{a}{\sqrt{2}\sigma}\right) - \text{Erf}\left(\frac{-a}{\sqrt{2}\sigma}\right)\right]}. \tag{12}$$

With this formula we can determine the gaussian cut factor using, cut ratio $= f_T(a)/A_T$, where cut ratio = 1/2 for a truncated Gaussian cut at FWHM.

Computing intensity profiles using the generated phase masks, we load each shaped beam profile into the 3D particle-in-cell code Impact-T [13] to quantify its emittance evolution. Impact-T includes both space-charge forces and short-range wakefields, and we use standard LCLS photoinjector settings (250 pC charge, nominal RF phase and solenoid focusing) to carry the beam through to the optical transition radiation (OTR) diagnostic screen. Comparing several transverse-laser shapes, we find that for LCLS-I parameters our phase-plate-shaped profile reduces the normalized rms emittance at OTR2 from 0.67 µm (typical virtual cathode profile) to 0.45 µm, a 33% improvement.

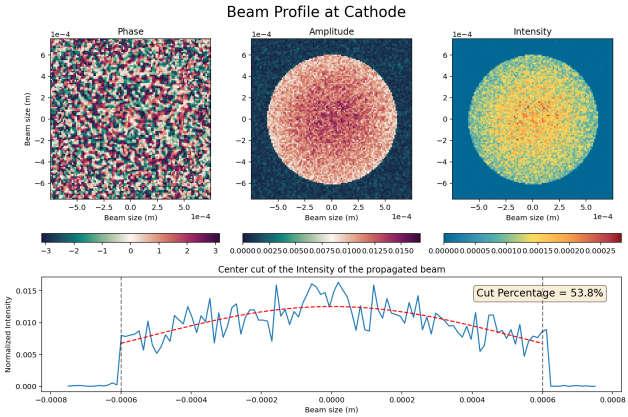

Figure 2: Simulated beam profile at the cathode using a phase plate generated for LCLS-I with 53.8% Gaussian cut.

EXPERIMENT AT FACET-II

Phase plate validation was carried out at the FACET-II photoinjector using the simple optical setup in Fig. 3. The drive laser was first expanded and collimated by a two-lens telescope, then transmitted through a commercial fused silica phase plate. A downstream converging lens propagated the beam so that the Fourier plane was at the photocathode.

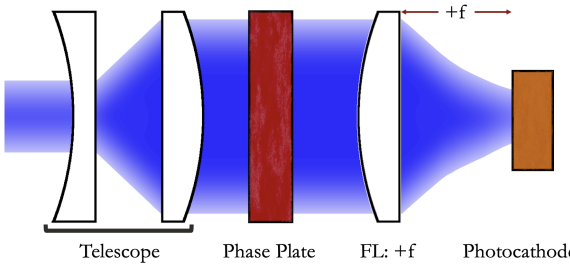

Figure 3: Schematic of phase plate setup for FACET-II photoinjector. The telescope ensures that the beam fills the phase mask aperture for correct performance.

Implementation at FACET-II (Fig. 4) shows an accurate transverse shaping where the cut ratio is 25.6 ± 0.2% and 22 ± 1% for the x and y projections respectively with a characteristic speckle of 67.5 µm.

Measurements also show a significant reduction in centroid jitter (Fig. 5) at the virtual cathode camera (VCC). The centroid jitter rms was reduced by 64% and 79% for the x and y directions respectively and the peak-to-peak was reduced by 61% and 74% for x and y respectively.
Along with this, the normalized emittance RMS was improved by 37% (from 5.4 µm to 3.4 µm) at 1.6 nC.

NANOFABRICATION

It was possible to confirm our simulations by fabricating a binary mask with 2 discrete phase levels [0, π]. The NanoX facility at SLAC was able to apply laser lithography [21] in order to fabricate a 1 inch diameter phase mask. The experimental results (Fig. 6) are shown below using a similar

ISBN: 978-3-95450-261-5 ISSN: 2673-7000 doi: 10.18429/JACoW-NAPAC2025-WEP092

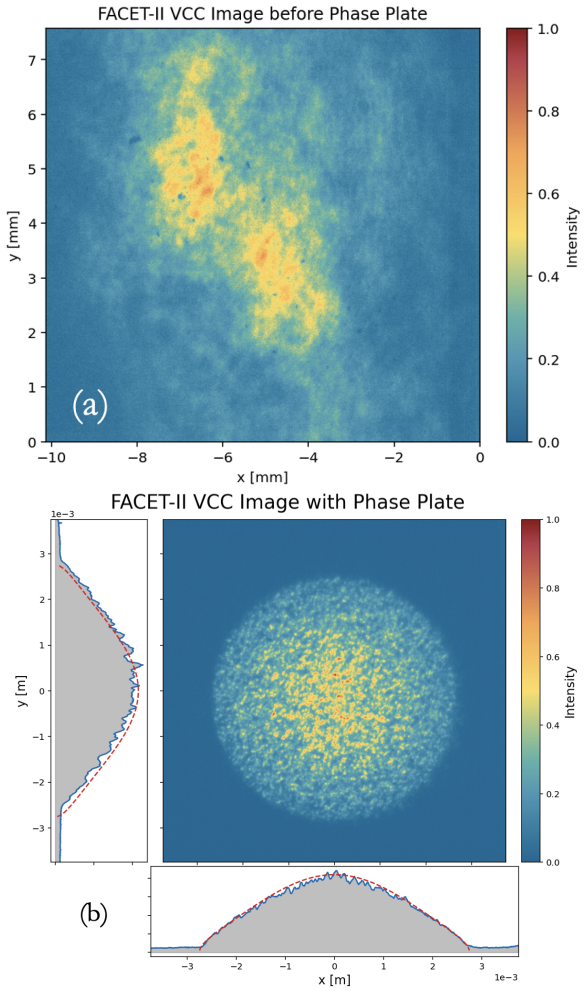

Figure 4: Laser transverse profile before (a) and after (b) implementing the phase plate at FACET-II.

Figure 5: Centroid jitter at the VCC for FACET-II before (blue) and after (orange) implementation of the phase plate. The data was de-trended to ignore effects due to room temperature variation.

setup (Fig. 3) that was put in place by FACET-II at LCLS-I. Here, the focal length used was 1.096 m for a phase mask generated for 1.2 m.

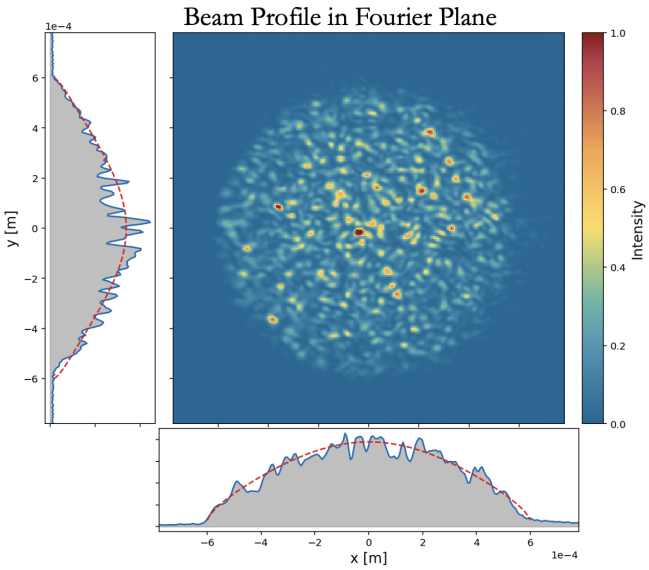

Figure 6: Experimental results of a 2-level phase plate fabricated at NanoX for LCLS-I.

The projection in x has a cut percentage of 38 ± 2% and the projection in y has a cut percentage of 23 ± 2%. We notice a large zeroth order intensity that could be due to the binary nature of the phase mask. The characteristic speckle was calculated using Eq. (10) to be 19.50 µm. We expect this profile to be improved through further developments.

CONCLUSION

By eliminating the power loss and UV incompatibility of conventional shaping methods, this approach enables stable, energy-efficient laser delivery and is fully compatible with the megahertz repetition rates envisioned for LCLS-II. These results establish phase-plate beam shaping as a scalable, high-fidelity tool for achieving low emittance and enhanced stability in high-brightness FEL photoinjectors. Future work will explore multi-level phase patterns, higher precision transverse machining and semi-random initial conditions [22] for IFTA to fabricate improved phase plates to enhance reliability of photoinjectors at LCLS.

ACKNOWLEDGEMENTS

This work is supported by U.S. Department of Energy Contract No. DE-AC02-76SF00515. The authors thank Tim Maxwell, Feng Zhou, Zhen Zhang, Christopher Mayes (ex-SLAC), Jingyi Tang, Zack Buschmann (SLAC) and Rachel Margraf-O'Neil, Philippe Piot (ANL) for useful discussion and feedback.

REFERENCES

[1] A. Halavanau *et al.*, "Spatial control of photoemitted electron beams using a microlens-array transverse-shaping technique", *Phys. Rev. Accel. Beams*, vol. 20, no. 10, p. 103 404, 2017. doi:10.1103/PhysRevAccelBeams.20.103404

ISBN: 978-3-95450-261-5 ISSN: 2673-7000 doi: 10.18429/JACoW-NAPAC2025-WEP092

[2] B. E. Carlsten, "New photoelectric injector design for the Los Alamos National Laboratory XUV FEL accelerator", *Nucl. Instrum. Methods Phys. Res., Sect. A*, vol. 285, no. 1-2, pp. 313–319, 1989. doi:10.1016/0168-9002(89)90472-5

[3] P. Emma *et al.*, "First lasing and operation of an ångstrom-wavelength free-electron laser", *Nat. Photon.*, vol. 4, no. 9, pp. 641–647, 2010. doi:10.1038/nphoton.2010.176

[4] K.-J. Kim, Z. Huang, and R. Lindberg, *Synchrotron radiation and free-electron lasers*. Cambridge, UK: Cambridge University Press, 2017. doi:10.1017/9781316677377

[5] S. Bettoni *et al.*, "Overview of swissfel dual-photocathode laser capabilities and perspectives for exotic fel modes", *High Power Laser Sci. Eng.*, vol. 9, p. e51, 2021. doi:10.1017/hpl.2021.36

[6] D. H. Dowell, *High brightness electron injectors for 4th generation light sources, lecture 1: Introduction and motivation*, USPAS Lecture Notes, Stanford Linear Accelerator Center, Menlo Park, CA, USA, 2010. https://uspas.fnal.gov/materials/10MIT/Lecture1_Intro_and_Motivation_text.pdf

[7] F. Zhou, A. Brachmann, P. Emma, S. Gilevich, and Z. Huang, "Impact of the spatial laser distribution on photocathode gun operation", *Phys. Rev. Spec. Top. Accel Beams*, vol. 15, no. 9, p. 090 701, 2012. doi:10.1103/PhysRevSTAB.15.090701

[8] D. Dowell *et al.*, "LCLS Drive Laser Shaping Experiments", in *Proc. FEL'09*, Liverpool, UK, Aug. 2009, pp. 463–465. https://jacow.org/FEL2009/papers/WEOA03.pdf

[9] C. Xu *et al.*, "Machine learning based spatial light modulator control for the photoinjector laser at FLUTE", in *Proc. IPAC'21*, Campinas, SP, Brazil, May 2021, pp. 3332–3335. doi:10.18429/JACoW-IPAC2021-WEPAB289

[10] C. Koschitzki *et al.*, "Chirped pulse laser shaping for high brightness photoinjectors", in *Proc. FEL'22*, Trieste, Italy, Aug. 2022, pp. 22–26. doi:10.18429/JACoW-FEL2022-WEAO4

[11] S. Li *et al.*, "Ultraviolet laser transverse profile shaping for improving x-ray free electron laser performance", *Phys. Rev. Accel. Beams*, vol. 20, no. 8, p. 080 704, 2017. doi:10.1103/PhysRevAccelBeams.20.080704

[12] J. R. Fienup, "Reconstruction of an object from the modulus of its Fourier transform", *Opt. Lett.*, vol. 3, no. 1, pp. 27–29, 1978. doi:10.1364/OL.3.000027

[13] J. Qiang, S. Lidia, R. D. Ryne, and C. Limborg-Deprey, "Three-dimensional quasistatic model for high brightness beam dynamics simulation", *Phys. Rev. Spec. Top. Accel Beams*, vol. 9, no. 4, p. 044 204, 2006. doi:10.1103/PhysRevSTAB.9.044204

[14] B. E. A. Saleh and M. C. Teich, *Fundamentals of Photonics, 2 Volume Set*. Hoboken, NJ: John Wiley & Sons, 2019. doi:10.1002/0471213748

[15] S. Serkez, J. Krzywinski, Y. Ding, and Z. Huang, "Soft x-ray self-seeding simulation methods and their application for the linac coherent light source", *Phys. Rev. Spec. Top. Accel Beams*, vol. 18, no. 3, p. 030 708, 2015. doi:10.1103/PhysRevSTAB.18.030708

[16] K. Khare, M. Butola, S. Rajora, *et al.*, *Fourier optics and computational imaging*. London, UK: Springer, 2015. doi:10.1007/978-3-031-18353-9

[17] G. Situ, "Deep holography", *Light: Advanced Manufacturing*, vol. 3, no. 2, pp. 278–300, 2022. doi:10.37188/lam.2022.013

[18] K. Wang *et al.*, "On the use of deep learning for phase recovery", *Light: Sci. Appl.*, vol. 13, no. 1, p. 4, 2024. doi:10.1038/s41377-023-01340-x

[19] C. Guo, S. Liu, and J. T. Sheridan, "Iterative phase retrieval algorithms. i: Optimization", *Appl. Opt.*, vol. 54, no. 15, pp. 4698–4708, 2015. doi:10.1364/AO.54.004698

[20] I. Hamarová, P. Šmíd, P. Horváth, and M. Hrabovský, "Methods for determination of mean speckle size in simulated speckle pattern", *Meas. Sci. Rev.*, vol. 14, no. 3, p. 177, 2014. doi:10.2478/msr-2014-0024

[21] S. Marchesini and A. Sakdinawat, "Shaping coherent x-rays with binary optics", *Opt. Express*, vol. 27, no. 2, pp. 907–917, 2019. doi:10.1364/OE.27.000907

[22] H. Pang, W. Liu, A. Cao, and Q. Deng, "Speckle-reduced holographic beam shaping with modified Gerchberg–Saxton algorithm", *Opt. Commun.*, vol. 433, pp. 44–51, 2019. doi:10.1016/j.optcom.2018.09.076